# Cosmological constraints without nonlinear redshift-space distortions

Mikhail M. Ivanov,[1,*] Oliver H. E. Philcox,[1,2,3] Marko Simonović,[4] Matias Zaldarriaga,[1]
Takahiro Nischimichi,[5,6] and Masahiro Takada[6]

[1]*School of Natural Sciences, Institute for Advanced Study, 1 Einstein Drive, Princeton, New Jersey 08540, USA*
[2]*Department of Astrophysical Sciences, Princeton University, Princeton, New Jersey 08540, USA*
[3]*Department of Applied Mathematics and Theoretical Physics, University of Cambridge, Cambridge CB3 0WA, United Kingdom*
[4]*Theoretical Physics Department, CERN, 1 Esplanade des Particules, Geneva 23, CH-1211, Switzerland*
[5]*Center for Gravitational Physics, Yukawa Institute for Theoretical Physics, Kyoto University, Kyoto 606-8502, Japan*
[6]*Kavli Institute for the Physics and Mathematics of the Universe (WPI), UTIAS The University of Tokyo, Kashiwa, Chiba 277-8583, Japan*

(Received 14 October 2021; accepted 27 January 2022; published 22 February 2022)

Nonlinear redshift-space distortions ("fingers of God") are challenging to model analytically, a fact that limits the applicability of perturbation theory (PT) in redshift space as compared to real space. We show how this problem can be mitigated using a new observable, $Q_0$, which can be easily estimated from the redshift-space clustering data and is approximately equal to the real-space power spectrum. The new statistic does not suffer from fingers of God and can be accurately described with PT down to $k_{\max} \simeq 0.4\ h\,\mathrm{Mpc}^{-1}$. It can be straightforwardly included in the likelihood at negligible additional computational cost and yields noticeable improvements on cosmological parameters compared to standard power spectrum multipole analyses. Using both simulations and observational data from the Baryon Oscillation Spectroscopic Survey, we show that improvements vary from 10% to 100% depending on the cosmological parameter considered, the galaxy sample, and the survey volume.

DOI: 10.1103/PhysRevD.105.043531

## I. INTRODUCTION

Reliable theoretical models for the intermediate- and short-scale galaxy power spectrum provide the key to obtaining tight constraints on cosmological parameters from current and future spectroscopic galaxy surveys [1–8]. In the analysis of the most recent Baryon Oscillation Spectroscopic Survey (BOSS) based on the Luminous Red Galaxy (LRG) sample [9], the main limiting factor in pushing to small scales is the nonlinear redshift-space distortions, also known as the "fingers of God" (FoG) [10]. These nonlinear effects contaminate the observed galaxy distribution along the line of sight $\hat{\mathbf{z}}$, even on relatively large scales. Further complications come from using the usual multipole expansion of the anisotropic redshift-space power spectrum, since it mixes modes that are parallel and perpendicular to $\hat{\mathbf{z}}$. As a result, FoG, which affect only the modes along the line of sight, leak into all power spectrum multipoles, significantly limiting the range of scales over which accurate modeling is possible.

In order to estimate the impact of FoG, it is instructive to compare the range of validity of a given power spectrum model in real and redshift space. Recent analyses of the realistic mock catalogs simulating the BOSS galaxy sample show that the one-loop redshift-space perturbation theory (PT) model breaks down at $k_{\max} \simeq 0.25\ h\,\mathrm{Mpc}^{-1}$ [3,11,12]. On the other hand, the real-space data for the same volume can be well described by the one-loop model up to significantly smaller scales, $k_{\max} \simeq 0.4\ h\,\mathrm{Mpc}^{-1}$ [13,14]. A similar picture was observed in the context of Lagrangian perturbation theory in Refs. [15–18]. While these results depend on the survey volume, the effective redshift, and the type of tracers observed, they suggest that there is a potential to improve measurements of cosmological parameters by isolating FoG and extracting the information from the transverse Fourier modes (perpendicular to $\hat{\mathbf{z}}$) that are not affected by the nonlinear redshift-space distortions.

Throughout the years, many methods had been proposed in order to achieve this goal. The most intuitive approach is to use the redshift-space power spectrum wedges [19,20]. In Fourier space, such techniques effectively operate at the

*ivanov@ias.edu

level of the anisotropic power spectrum $P(k,\mu)$, where $\mu \equiv \hat{\mathbf{k}} \cdot \hat{\mathbf{z}}$, and allow one to use a $\mu$-dependent $k_{\rm max}$ in the analysis [20]. While conceptually simple, the main shortcoming of wedges is that they cannot be efficiently estimated using fast Fourier transform (FFT) techniques, and in practice, one has to estimate "pseudowedges," obtained from the standard power spectrum multipoles [20]. Alternatively, several prescriptions have been used to "remove" FoG directly at the map level [21–23], but it remains unclear if the additional systematic errors produced by such methods produce are too large for current and upcoming spectroscopic surveys [23].

In this paper, we build upon ideas from older works [21,22,24,25] and use a simple alternative statistic, dubbed $Q_0$. This is closely related to the real-space power spectrum and achieves the goal of isolating the FoG. In essence, this is obtained by measuring a particular linear combination of the first few power spectrum multipoles. The main advantages of $Q_0$ are the following:

(a) It can be easily measured using conventional power spectrum multipole estimators.
(b) Modulo small effects induced by the broadening of the baryon acoustic oscillation (BAO) peak that affect only the BAO wiggles, $Q_0$ is equal to the real-space power spectrum and can be modeled to higher $k_{\rm max}$.
(c) Its covariance matrix can be straightforwardly computed either analytically or from mock catalogs. $Q_0$ can thus be easily included in the galaxy power spectrum likelihood at negligible extra cost, opening up the possibility to partially include additional small-scale information and improve cosmological constraints compared to conventional power spectrum multipole analyses.

Before we dive into the details, it is worth pointing out the main difference in our approach compared to all previous work, which is related to reliably estimating the covariance for $Q_0$. The problem arises from the fact that the nonlinear clustering generates all possible multipoles, whose covariance rapidly increases with the multipole order, $\ell$. Therefore, if one attempts to produce a better estimate of the real-space power spectrum using information from higher and higher $\ell$, the estimator quickly becomes very noisy and essentially contains no information. This is clearly a paradox. In this work, we show how to resolve this issue and estimate $Q_0$ in a systematic fashion, while keeping the covariance under control. Our method is based on the theoretical error covariance approach [26,27]. The key idea is to impose natural priors on the smoothness of the higher-order multipoles, which, as we will show, effectively suppresses their contribution to the covariance of $Q_0$, while still contributing to the statistic itself. This approach allows multipoles up to arbitrary $\ell_{\rm max}$ to be included in the analysis if needed, guaranteeing the optimal error bars on $Q_0$.

Our paper is organized as follows. We begin with a preliminary discussion in Sec. II, showing how $Q_0$ can be built from the usual Legendre multipoles with $\ell_{\rm max} = 4$, and discuss its relation to the real-space power spectrum. Our approach is generalized to the case of general $\ell_{\rm max}$ in Sec. III. Validation on large-volume N-body simulation data is given in Sec. IV, and applications to the real BOSS data and the DESI-like mocks are shown in Sec. V. Finally, we draw conclusions in Sec. VI. Some additional material is presented in Appendix.

Throughout most of this paper, we will use the PT challenge simulation data [11], comprising BOSS-like mock catalogs with cumulative volume $\sim 566\ ({\rm Gpc}/h)^3$. We use a combination of ten independent simulation boxes with side length $L = 3840\ {\rm Mpc}/h$ and $3072^3$ particles each. For our purposes, we use only a single redshift bin with $z = 0.61$. We will describe the data from the mocks using one-loop perturbation theory templates, as implemented in the CLASS-PT code [14]. The parameter constraints are obtained with the MONTEPYTHON Markov chain Monte Carlo (MCMC) sampler [28,29] and analyzed using the GetDist package [30].

## II. PRELIMINARY ANALYSIS

It is instructive to begin with a simplified example whereupon $P(k,\mu)$ is fully characterized by its first four moments, just as in linear theory [31]. In this instance, there is a simple rotationlike transformation between the moments of $\mu$ and the Legendre multipoles $P_\ell$,

$$P(k,\mu) = \sum_{\ell=0,2,4} P_\ell(k)\mathcal{L}_\ell(\mu) = \sum_{n=0,2,4} Q_n(k)\mu^n, \quad (2.1)$$

where $\mathcal{L}_\ell$ is the Legendre polynomial of order $\ell$. The power spectrum perpendicular to the line of sight, i.e., at $\mu = 0$, is given by $Q_0$. By definition, this coincides with the real-space galaxy power spectrum, which can be well described by the one-loop PT model up to $k_{\rm max} \sim 0.4\ h\,{\rm Mpc}^{-1}$ [13]. In contrast, the one-loop PT model for $Q_2$ and $Q_4$ breaks down on larger scales, since these moments are dominated by FoG [3,11,14]. FoG are a strong UV effect that lowers the cutoff of the redshift-space effective field theory [32–34]. Indeed, estimates from the BOSS LRG sample give a redshift-space cutoff [1],

$$k_{\rm NL,FoG} \approx \sigma_v^{-1} \simeq 0.25\ h\,{\rm Mpc}^{-1}, \quad (2.2)$$

where $\sigma_v$ is the short-scale velocity dispersion. This can be contrasted with the cutoff of the real-space effective field theory $k_{\rm NL,rs}$ (see Refs. [27,35,36]), which Ref. [26] estimates to be

$$k_{\rm NL,rs} \simeq 0.5\ h\,{\rm Mpc}^{-1}. \quad (2.3)$$

Our goal is to extract the information contained in $Q_0$ while marginalizing over $Q_2$ and $Q_4$. An important problem is that the quantities measured by standard FFT power spectrum estimators are the multipoles (see, e.g., Refs. [37–39]) and not the moments of $\mu$. The multipoles pick up contributions from all moments, including those affected by FoG, i.e.,

$$P_0 = Q_0 + \frac{1}{3}Q_2 + \frac{1}{5}Q_4, \quad P_2 = \frac{2}{3}Q_2 + \frac{4}{7}Q_4, \quad P_4 = \frac{8}{35}Q_4. \tag{2.4}$$

However, given these simple linear relations, one can easily construct an estimator for $Q_0$ from the multipole estimators. Indeed, a straightforward estimator for $Q_0$ is given by the usual Scoccimarro-Yamamoto formula [38],

$$\begin{aligned}\check{Q}_0(k_i) &= \check{P}_0 - \frac{1}{2}\check{P}_2 + \frac{3}{8}\check{P}_4 \\ &= \frac{1}{V}\int_{k_i}\frac{d^3k}{4\pi k_i^2\Delta k}\delta_0\bigg((2\cdot 0+1)\delta_0 - \frac{(2\cdot 2+1)}{2}\delta_2 \\ &\quad + \frac{3(2\cdot 4+1)}{8}\delta_4\bigg),\end{aligned} \tag{2.5}$$

where $V$ is the survey volume and $\int_{k_i}$ is the integral over the momentum shell of width $\Delta k$ which is centered at $k_i$. Moreover, we have assumed the flat-sky approximation and the Kaiser limit [31] for the local redshift-space overdensity $\delta_\ell$, weighted with the appropriate Legendre polynomials,

$$\delta_\ell(k,\mu) \equiv (b_1 + f\mu^2)\delta_{\rm lin}(k)\mathcal{L}_\ell(\mu). \tag{2.6}$$

In practice, if the measurements of $P_{0,2,4}$ are available, $Q_0$ can be constructed from this data vector by a simple linear summation of these multipoles with appropriate coefficients. The covariance matrix for $Q_0$ can be obtained directly from the estimator (2.5),

$$\begin{aligned}&\langle\check{Q}_0(k_i)\check{Q}_0(k_j)\rangle - \langle\check{Q}_0(k_i)\rangle\langle\check{Q}_0(k_j)\rangle \\ &= \frac{(2\pi)^3\delta_{ij}}{V4\pi k_i^2\Delta k}\int_0^1 d\mu\, P(k_i)^2(b_1+f\mu^2)^4\bigg(\mathcal{L}_0(\mu) - \frac{2\cdot 2+1}{2}\mathcal{L}_2(\mu) + \frac{3}{8}(2\cdot 4+1)\mathcal{L}_4(\mu)\bigg)^2 \\ &= \frac{(2\pi)^3\delta_{ij}}{V4\pi k_i^2\Delta k}\bigg(\frac{225\check{P}_0^2}{64} - \frac{225\check{P}_0\check{P}_2}{88} + \frac{3775\check{P}_0\check{P}_4}{2288} + \frac{6975\check{P}_2^2}{9152} - \frac{775\check{P}_2\check{P}_4}{1144} + \frac{54975\check{P}_4^2}{155584}\bigg).\end{aligned} \tag{2.7}$$

Note that $P_0$ in the above formula contains the stochastic shot-noise term, equal to the inverse number density $\bar{n}^{-1}$ in the Poisson limit. The leading contribution to the covariance is given by the monopole moment (including the shot noise),

$$\frac{2}{N_k}\frac{225P_0^2}{64} \simeq \frac{2}{N_k}3.5P_0^2, \tag{2.8}$$

which is 3.5 times larger than the (auto)covariance on the monopole and ∼4 times larger than the real space covariance (the additional increase is due to the Kaiser effect [31]). This apparent inflation of the error bars is driven by higher-order multipoles $P_2$ and $P_4$, which are characterized by a large covariance. Thus, the large error on the reconstructed transverse moment $Q_0$ is the inevitable price of using the noisy Legendre multipoles in the estimator.

Alternatively, one can obtain the covariance matrix for $Q_0$ directly from the covariance matrix of the multipoles by an orthogonal transformation dictated by Eq. (2.4). Denoting this transformation as $P_\ell = M_{\ell n}Q_n$ (assuming Einstein summation conventions), we obtain

$$\begin{aligned}\hat{C}_{00}^{(Q)} &= [(\hat{M}^T)_{0\ell} * \hat{C}^{-1}_{\ell\ell'} * \hat{M}_{\ell' 0}]^{-1} \\ &= \hat{C}_{00} - \hat{C}_{02} + \frac{3\hat{C}_{04}}{4} + \frac{\hat{C}_{22}}{4} - \frac{3\hat{C}_{24}}{8} + \frac{9\hat{C}_{44}}{64},\end{aligned} \tag{2.9}$$

which reduces to Eq. (2.7) in the Gaussian approximation. For a realistic survey, the covariance of $Q_0$ can also be estimated from mock catalogs with the usual empirical estimator.

Let us consider the $Q_n$ moments extracted from the PT challenge data, as shown in Fig. 1. Note that the PT challenge redshift-space power spectrum moments $P_\ell$ are modulated by the Alcock-Paczynski (AP) effect [40], which is absent in the actual real-space power spectrum $P_{gg}$, for which the comoving distances are computed using the true cosmology. In order to account for the difference between $Q_0$ and $P_{gg}$, we rescale the latter by the isotropic AP factor. As expected, we see that $Q_0$ is almost identical to the real-space power spectrum, once the AP effect is taken into account (see also Fig. 8 from an earlier work [25]). However, the higher moments $Q_n$ vary quite significantly on mildly nonlinear scales. In particular, $Q_2$ crosses zero at $k \simeq 0.3\ h\,{\rm Mpc}^{-1}$, which may be interpreted as the PT breakdown for these moments; the zero-crossing means that the nonlinear correction is comparable to the linear one. Moreover, nonlinearities in the velocity field generate higher-order multipoles with $\ell > 4$. We show these multipoles (up to $\ell = 8$) estimated from the PT challenge data in the bottom panel of Fig. 1. In the presence of higher-order power spectrum multipoles, the estimator for $Q_0$ is given by (see Appendix for a derivation)

$$\check{Q}_0 = \check{P}_0 - \frac{1}{2}\check{P}_2 + \frac{3}{8}\check{P}_4 - \frac{5}{16}\check{P}_6 + \frac{35}{128}\check{P}_8 + \cdots \tag{2.10}$$

In the next section, we introduce a general formalism that allows one to take higher-order multipoles into account consistently.

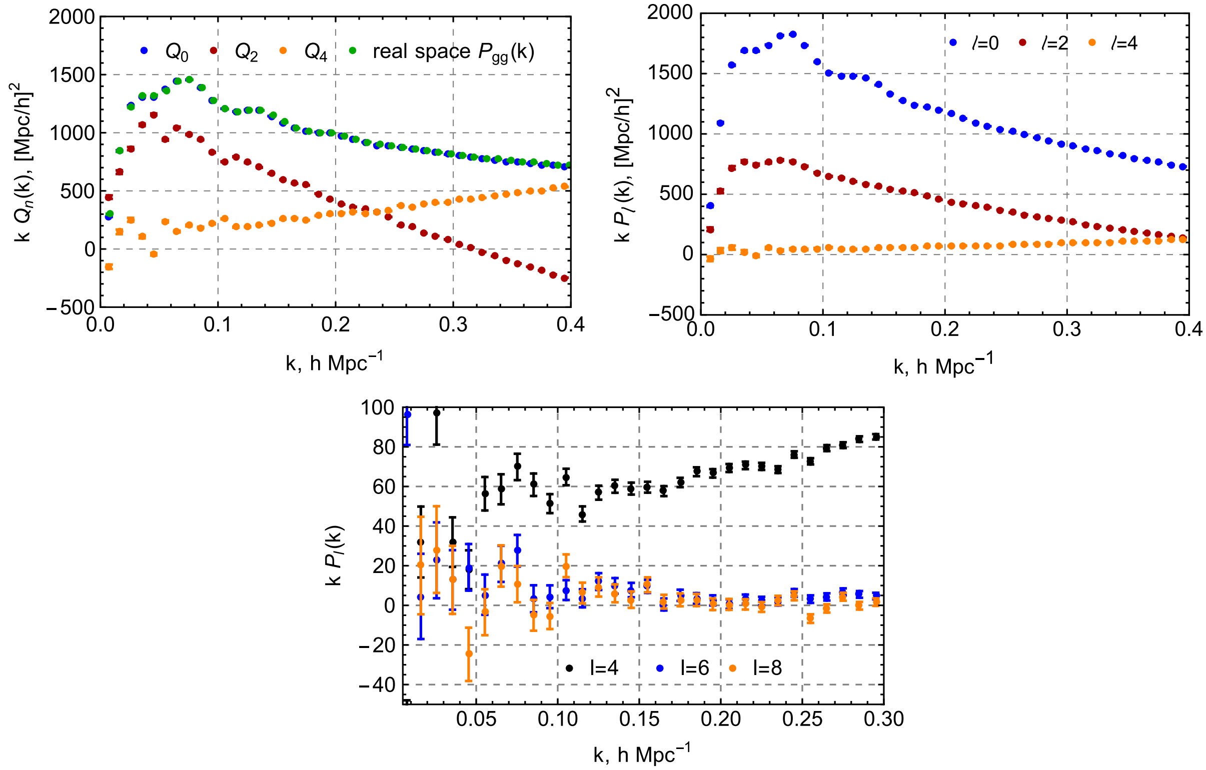


FIG. 1. Upper panel: comparison of moments, $Q_n$, and multipoles, $P_\ell$, for the redshift-space power spectrum of PT challenge galaxies. The real-space power spectrum $P_{gg}$ (rescaled to match the AP effect present in $Q_0$) in the left plot is slightly shifted horizontally for clarity, as the data points overlap with those of $Q_0$. Lower panel: higher-order Legendre multipoles with $\ell = 4, 6, 8$.

## III. FORMAL DERIVATION

In this section, we will present a general formalism that allows one to reconstruct $Q_0$ from any survey for arbitrary $\ell_{\max}$. We saw in the previous section that using large $\ell_{\max}$ in the estimator of $Q_0$ leads to the inflation of the statistical errors since higher-order Legendre multipoles have larger variances. However, one can imagine a situation in which the survey volume is such that these moments can become important, and their exclusion can lead to noticeable systematic errors. To include $Q_0$ for an arbitrary $\ell_{\max}$, it is more convenient to rederive the previous results using a different approach, which we present here.

### A. Case of $\ell_{\max} = 4$

Let us start again with the familiar case $\ell_{\max} = 4$ and consider the likelihood for power spectrum multipoles in the Gaussian diagonal approximation,

$$
\begin{aligned}
&-2\ln L(Q_0, Q_2, Q_4) = \Delta\vec{P}_\ell \cdot \hat{C}^{-1}_{\ell\ell'} \cdot \Delta\vec{P}_{\ell'}, \quad \text{where} \\
&\Delta\vec{P}_0 = \left(Q_0(k_i) + \frac{1}{3}Q_2(k_i) + \frac{1}{5}Q_4(k_i) - P_0^{\text{data}}(k_i)\right), \\
&\Delta\vec{P}_2 = \left(\frac{2}{3}Q_2(k_i) + \frac{4}{7}Q_4(k_i) - P_2^{\text{data}}(k_i)\right), \\
&\Delta\vec{P}_4 = \left(\frac{8}{35}Q_4(k_i) - P_4^{\text{data}}(k_i)\right),
\end{aligned}
\tag{3.1}
$$

where we have suppressed the explicit summation over multipoles and and wave number indices.

In the Gaussian approximation, all $k$-bins are independent. Thus, we can consider the likelihood for each bin separately. Marginalizing the likelihood (3.1) for the $i$th bin over $Q_2$ and $Q_4$, we obtain we following reduced likelihood,[1]

$$
-2\ln L_{\text{marg}}(Q_0) = \sum_{i=1}^{N_{\text{bins}}} \frac{(P_0^{\text{data}}(k_i) - \frac{1}{2}P_2^{\text{data}}(k_i) + \frac{3}{8}P_4^{\text{data}}(k_i) - Q_0(k_i))^2}{C_{00} - C_{02} + \frac{3C_{04}}{4} + \frac{C_{22}}{4} - \frac{3C_{24}}{8} + \frac{9C_{44}}{64}}, \tag{3.2}
$$

[1]For simplicity, we will ignore the logarithmic corrections to the marginalization result in what follows. The leading effect of these corrections is to change the likelihood normalization, which can be neglected in MCMC analysis.

which exactly coincides with the likelihood for $Q_0$ from the previous section. Clearly, this derivation has allowed too much freedom; we have marginalized over $Q_2$ and $Q_4$, allowing independent and arbitrarily large fluctuations in every $k$-bin. However, we expect that the scale-dependent FoG contributions are smooth finite functions. This condition can be implemented by means of the prior on the (unknown) full theoretical model, along the lines of Ref. [26].

### B. Warm-up: Theoretical prior on the quadrupole

Next, let us discuss how the likelihood for $Q_0$ changes if we include some prior information on the power spectrum multipoles. Our derivation will closely follow the derivation of the covariance matrix in the theoretical error formalism [26]. For simplicity, let us consider a situation in which the redshift-space power spectrum depends only on the two moments, $Q_0$ and $Q_2$. We need to marginalize this likelihood over $Q_2$. Repeating the derivation above, we find following likelihood for $Q_0$ alone:

$$-2\ln L(Q_0) = \sum_{i=1}^{N_{\rm bins}} \frac{(P_0^{\rm data}(k_i) - P_2^{\rm data}(k_i)/2 - Q_0(k_i))^2}{C_{00}(k_i) - C_{02}(k_i) + C_{22}(k_i)/4}. \tag{3.3}$$

We now assume that there is some prior knowledge of the expectation value $\overline{P}_2$ with some error $E_i$. In other words, there is a likelihood for the theoretical prediction of $\bar{P}_2$,

$$\begin{aligned} -2\ln L_{\rm E} &= (P_2[Q_2] - \bar{P}_2)\cdot \hat{C}^{-1}_{(P_2)}\cdot (P_2[Q_2] - \bar{P}_2) = (\Delta\vec{Q}_2 - \Delta\vec{Q}_2')\cdot \hat{\Psi}^{(E)}\cdot (\Delta\vec{Q}_2 - \Delta\vec{Q}_2'),\\ \Delta\vec{Q}_2 &= \vec{Q}_2 - \vec{Q}_2^{\rm data}, \qquad \Delta\vec{Q}_2' = \vec{\bar{Q}}_2 - \vec{Q}_2^{\rm data}, \end{aligned} \tag{3.4}$$

where the second equality has rewritten the likelihood for $P_2$ in terms of the likelihood for $Q_2$, using $\bar{Q}_2 \equiv 3\bar{P}_2/2$ and defining some precision matrix $\hat{\Psi}^{(E)}$. The split into $\Delta\vec{Q}_2$ and $\Delta\vec{Q}_2'$ will be clear shortly. Note that, in principle, the covariance $C^{-1}_{(P_2)}$ is fully correlated. The total likelihood takes the following form:

$$\begin{aligned} -2\ln L(Q_0, Q_2) &= \sum_{i=1}^{N_{\rm bins}} \Delta\vec{P}_\ell C^{-1}_{\ell\ell'}\Delta\vec{P}_{\ell'} + \sum_{i,j}^{N_{\rm bins}} C_E^{-1}(P_2[Q_2](k_i) - \overline{P}_2(k_i))(P_2[Q_2](k_j) - \bar{P}_2(k_j)),\\ &= \Delta\vec{Q}_m\cdot\hat{\Psi}_{mn}\cdot\Delta\vec{Q}_n + \Delta\vec{Q}_2\cdot\hat{\Psi}^{(E)}\cdot\Delta\vec{Q}_2. \end{aligned} \tag{3.5}$$

The likelihood marginalized over $Q_2$ can be easily obtained,

$$\begin{aligned} -2\ln L(Q_0) &= (\Delta\vec{Q}_0 + \{\hat{\Psi}_{00} - \hat{\Psi}_{02}(\hat{\Psi}_{22} + \hat{\Psi}^{(E)})^{-1}\hat{\Psi}_{02}\}^{-1}(\hat{\Psi}_{02}(\hat{\Psi}_{22} + \hat{\Psi}^{(E)})^{-1}\hat{\Psi}^{(E)}\cdot\Delta\vec{Q}_2'))\\ &\quad\times(\hat{\Psi}_{00} - \hat{\Psi}_{02}(\hat{\Psi}_{22} + \hat{\Psi}^{(E)})^{-1}\hat{\Psi}_{02})\\ &\quad\times(\Delta\vec{Q}_0 + \{\hat{\Psi}_{00} - \hat{\Psi}_{02}(\hat{\Psi}_{22} + \hat{\Psi}^{(E)})^{-1}\hat{\Psi}_{02}\}^{-1}(\hat{\Psi}_{02}(\hat{\Psi}_{22} + \hat{\Psi}^{(E)})^{-1}\hat{\Psi}^{(E)}\cdot\Delta\vec{Q}_2')). \end{aligned} \tag{3.6}$$

To obtain some insight into the structure of this likelihood, we use several approximations. First, let us neglect the cross-covariance $C_{02}$ between the multipoles; this is reasonable since the normalized correlation coefficient is typically small, $r_{02} = C_{02}/(C_{00}^{1/2}C_{22}^{1/2}) \sim 0.1 \ll 1$ for the PT challenge mocks. Note that the prediction matrix is not diagonal; i.e., $\hat{\Psi}_{02}$ is still nontrivial in this approximation, with

$$\hat{\Psi}_{02} = \hat{C}_{00}^{-1}/3. \tag{3.7}$$

As a second approximation, we consider the asymptotic regime $C_E/C \to \infty$. This corresponds to very poor prior knowledge about $\bar{P}_2$. In this limit, the terms with the theoretical error drop out, and to leading order in $\mathcal{O}((C_E/C)^{-1})$, we obtain

$$\begin{aligned} -2\ln L(Q_0) &= (P_0^{\rm data} - P_2^{\rm data}/2 - Q_0)\cdot(\hat{\Psi}_{00} - \hat{\Psi}_{02}\hat{\Psi}_{22}^{-1}\hat{\Psi}_{02})\cdot(P_0^{\rm data} - P_2^{\rm data}/2 - Q_0)\\ &= \sum_{i=1}^{N_{\rm bins}} \left.\frac{(P_0^{\rm data} - P_2^{\rm data}/2 - Q_0)^2}{C_{00} + C_{22}/4}\right|_{k_i}, \end{aligned} \tag{3.8}$$

where in the last line we have implemented the Gaussian approximation. Equation (3.8) gives a usual likelihood with the variance on the estimator $\hat{Q}_0 = P_0 - P_2/2$ reconstructed from the monopole and the quadrupole. In the opposite limit $C_E/C \to 0$, where the theoretical prior is infinitely precise, we have

$$-2\ln L(Q_0) = \sum_{i=1}^{N_{\rm bins}} \frac{(Q_0 - P_0^{\rm data} + \bar{P}_2/2)^2}{C_{00}} + \mathcal{O}(C_E). \quad (3.9)$$

As expected, at leading order in $C^{(E)}$, adding the prior knowledge on $P_2$ is analogous to fitting the $Q_0$ moment constructed with the prior prediction $\bar{P}_2$, i.e.,

$$\hat{Q}_0 = P_0 - \frac{1}{2}\bar{P}_2. \quad (3.10)$$

Importantly, in this case, one does not pay the price of including (noisy) $P_2$ in the estimator for $\hat{Q}_0$; i.e., the covariance is given only by the monopole contribution.

### C. Generalization to higher-order multipoles

Generalization is straightforward and takes the form

$$\begin{aligned} &-2\ln L(Q_0, \ldots, Q_{\ell_{\max}}) \\ &= \sum_{i=1}^{N_{\rm bins}} \sum_{\ell,\ell' \le \ell_{\max}} C^{-1}_{\ell\ell' \rm data} \Delta P_\ell \Delta P_{\ell'} \\ &\quad + \sum_{\ell=0}^{\ell_{\max}} \sum_{i,j}^{N_{\rm bins}} (P_\ell[Q](k_i) - \bar{P}_\ell(k_i)) \\ &\quad \times (\hat{C}^{({\rm E}),(\ell\ell')})^{-1}_{ij} (P_\ell[Q](k_j) - \bar{P}_\ell(k_j)), \end{aligned} \quad (3.11)$$

where $P_\ell[Q]$ denotes a general expression for the power spectrum multipole $\ell$ through moments of $\mu$ (see Appendix). The prior $\bar{P}_\ell$ can be either a fit to the data with some smooth function or taken from the perturbation theory prediction. For $\ell > 4$, either option gives an envelope very close to 0 on mildly nonlinear scales. The final likelihood for $Q_0$ is obtained by marginalizing (3.11) over all $Q_\ell$ functions with $\ell \ge 2$, which can be performed analytically. In general, smoothness in $\mu$ and $k$ implies that the prior covariance should be 100% correlated [14]:

$$C_{ij}^{({\rm E}),(\ell\ell')} = E_\ell(k_i) E_{\ell'}(k_j). \quad (3.12)$$

However, given that the true shape is not known, we impose a weaker condition on smoothness in $\mu$ and $k$-space. Namely, we will use [27]

$$\begin{aligned} C_{ij}^{({\rm E}),(\ell\ell')} &= E_\ell(k_i) E_{\ell'}(k_j) \exp\left(-\frac{(k_i - k_j)^2}{2\Delta k^2}\right) \\ &\quad \times \exp\left(-\frac{(\ell - \ell')^2}{2\Delta \ell^2}\right). \end{aligned} \quad (3.13)$$

Conservatively, we can choose the theory prior to be 100% of the expected value, e.g.,

$$E_\ell(k_i) = \bar{P}_\ell(k_i). \quad (3.14)$$

The full likelihood (3.11) simplifies in the two extreme limits, $C_E \ll C_{\rm data}$ and $C_E \gg C_{\rm data}$. As we have seen in the previous section, in the first case, one needs to simply replace the true data vector $P_\ell$ by $\bar{P}_\ell$ in the estimator of $\hat{Q}_0$. This does not require any change to the covariance; hence, we do not pay the price of using the noisy $P_\ell$ in our $Q_0$ estimator. In the second case, we must use the $P_\ell$ from the data when constructing $\hat{Q}_0$ and include the noise of this multipole in our covariance. For all practical purposes, it is sufficient to work within these two limits. To estimate the transition between the two regimes, we may compare the effective $\chi^2$ contribution coming from the data and the prior on $P_\ell$:

$$\begin{aligned} \chi^2_{\rm data} &= (\vec{P}_\ell - \vec{\bar{P}}_\ell) \cdot \hat{C}^{-1}_{\ell\ell} \cdot (\vec{P}_\ell - \vec{\bar{P}}_\ell) \\ \chi^2_{\rm prior} &= (\vec{P}_\ell - \vec{\bar{P}}_\ell) \cdot (\hat{C}^{(E)}_{(\ell\ell')})^{-1} \cdot (\vec{P}_\ell - \vec{\bar{P}}_\ell). \end{aligned} \quad (3.15)$$

This suggests the following algorithm to deal with multipoles $\ell \ge 4$:

(1) Select some $\ell_{\max} \ge 4$, and estimate all mutipoles with $\ell \le \ell_{\max}$. Fit these multipoles with some smooth curves $\bar{P}_\ell$.
(2) For each $4 \le \ell \le \ell_{\max}$ compute the ratio $\chi^2_{\rm data}/\chi^2_{\rm prior}$. If $\chi^2_{\rm data}/\chi^2_{\rm prior} > 1$, $P_\ell$ should be included in the $Q_0$ estimator along with its effect on the covariance. In the opposite regime, $\check{Q}_0$ and its covariance should be estimated using only the lower multipoles. For all higher multipoles, add the contribution from the relevant multipole moment $\ell$ as a smooth prior $\bar{P}_\ell$ to $\check{Q}_0$.

### D. Modeling $Q_0$

Finally, let us discuss the theoretical model for $Q_0$. In linear theory, $Q_0$ would be the real-space galaxy auto power spectrum $P_{\rm gg}$. The situation becomes more complicated when IR resummation (i.e., the effects of long-wavelength displacements, which cannot be treated perturbatively) is taken into account. Indeed, the nonlinear BAO damping factor is direction dependent [41]. Assuming a wiggly/smooth decomposition of the linear power spectrum $P_{\rm lin} = P_{\rm nw} + P_{\rm w}$ [42–45], at leading order, we may write

$$P(k,\mu) = (b_1 + f\mu^2)^2 \times (P_{\rm nw} + P_{\rm w} e^{-\Sigma^2 k^2 (1+f\mu^2(2+f)) - \delta\Sigma^2 k^2 f^2 \mu^2 (\mu^2 - 1)}), \tag{3.16}$$

where the BAO damping functions are given by

$$\Sigma^2 = \frac{1}{6\pi^2}\int_0^{k_S} dq\, P_{\rm nw}(q)(1 - j_0(qr_{\rm BAO}) + 2j_2(qr_{\rm BAO})),$$
$$\delta\Sigma^2 = \frac{1}{2\pi^2}\int_0^{k_S} dq\, P_{\rm nw}(q) j_2(qr_{\rm BAO}), \tag{3.17}$$

for spherical Bessel functions $j_\ell(x)$, comoving BAO scale at the drag epoch $r_{\rm BAO}$, and separation scale $k_S$. Since the damping factor is large, the exponential suppression cannot be Taylor expanded. This means, that, in general, we need to use an infinite series in $P_\ell$ in our estimator of $Q_0$ in order to remove the direction dependence of the BAO wiggles. However, as the shape of the BAO wiggles is known analytically to all orders in $\mu$, we can just compute redshift-space multipoles, $\{P_\ell\}$, theoretically and then combine them into $Q_0$ just as for the data. This guarantees that the suppression of the BAO wiggles in $Q_0$ is the same in the data vector and in the theory model. Thus, our theory model is

$$Q_0(k) = P_0(k) - \frac{1}{2}P_2(k) + \frac{3}{8}P_4(k), \tag{3.18}$$

where $P_{0,2,4}$ contain all necessary redshift-space counterterms. The priors on these counterterms can be extracted from fitting the full data vector $P_{0,2,4}$ at low $k_{\rm max}$, where the perturbative modeling of FoG is still accurate.

## IV. VALIDATION ON PT CHALLENGE MOCKS

In this section, we apply the formalism described above to the PT challenge data. We will use the Gaussian approximation for all sample covariance matrices, which has been shown to be very accurate for the purpose of parameter constraints [46].

### A. Estimation of $Q_0$ from the data

As a first step, we obtain an estimate for $\bar{P}_\ell$ from the fits to the data, as in the left panel of Fig. 2. As a second step, we compute $\chi^2_{\rm data}/\chi^2_{\rm prior}$, assuming the following 100% prior on $P_\ell$:

$$C_{ij}^{({\rm E})\,(\ell\ell')} = \bar{P}_\ell(k_i)\bar{P}_{\ell'}(k_j)\exp\left(-\frac{(k_i-k_j)^2}{2\Delta k^2}\right) \times \exp\left(-\frac{(\ell-\ell')^2}{2\Delta\ell^2}\right). \tag{4.1}$$

The coherence length $\Delta k$ characterizes the amount of correlation across different $k$-bins and ensures that the

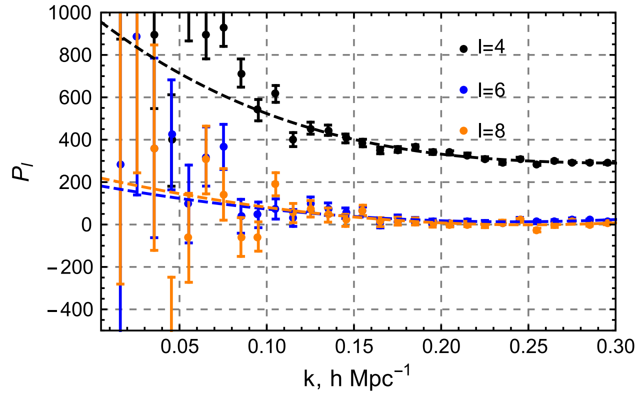


FIG. 2. Higher-order multipoles of the PT challenge data and their fits by quadratic polynomials.

likelihood properties do not depend on the binning. Choosing a large $\Delta k$ increases the significance of the theoretical prior by assuming an extra correlation between $k$-bins. The coherence in $\ell$ space corresponds to a smoothness of the power spectrum as a function of $\mu$. In practice, we choose $\Delta k = 0.001\ h/{\rm Mpc}$ and assume also that the theoretical prior covariance matrix is diagonal in the multipole space, i.e., $\Delta\ell = 0$. This choice corresponds to a very conservative situation where the prior on $\bar{P}_\ell$ is quite poor. Essentially, we do not require the two-dimensional power spectrum prior $P(k,\mu)$ to be a smooth function in both $k$ and $\mu$. Even this very conservative situation will be sufficient for our purposes. With our choice of $\Delta k$ and $\Delta\ell$, and using $k_{\rm max} = 0.3\ h/{\rm Mpc}$, we find

$$\frac{\chi^2_{\rm prior}}{\chi^2_{\rm data}} = 0.9,\ 80,\ 75 \quad \text{for } \ell = 4,\ 6,\ 8. \tag{4.2}$$

One can also check that $\chi^2_{\rm prior}/\chi^2_{\rm data} \ll 1$ is always true for $\ell = 0,\ 2$. For a more aggressive choice of $\Delta k = 0.01\ h\,{\rm Mpc}^{-1}$, we obtain the following numbers,

$$\frac{\chi^2_{\rm prior}}{\chi^2_{\rm data}} = 2,\ 232,\ 196 \quad \text{for } \ell = 4,\ 6,\ 8, \tag{4.3}$$

which do not change results qualitatively. These results suggests that our prior is marginally important for $\ell = 4$, and it is much more significant than the actual likelihood contribution for $\ell > 4$. If we include off-diagonal-in-$\ell$ matrix elements, which correspond to a prior on the smoothness of the power spectrum in $\mu$, the significance of the priors will increase even further. In particular, for $\Delta\ell = 2$, we have

$$\frac{\chi^2_{\rm prior}}{\chi^2_{\rm data}} = 3.3,\ 152 \quad \text{for } \ell = 4,\ 6. \tag{4.4}$$

On the one hand, the $\ell = 4$ prior never dominates over the data by more than a factor of few, regardless of the setup. To be maximally conservative, we will always include the hexadecapole in our analysis and take into account its contribution into the covariance matrix. On the other hand, we see that the contribution of higher order multipoles ($\ell > 4$) is always dominated by priors. Thus, we conclude that, even for the large-volume PT challenge mocks, the higher-order multipole moments $\ell > 4$ can be ignored in the estimation of the covariance matrix for $Q_0$ in the mildly nonlinear regime. However, we may want to include higher multipoles in the form of the mean prior to the theoretical model. To this end, we need to check if their inclusion is strictly needed to describe the data. To that end, we perform several MCMC analyses of the $Q_0$ likelihood from the PT challenge data for different choices of $\ell_{\max}$.

We fit the joint likelihood comprising the multipoles $P_{0,2,4}$ for $k_{\max} = 0.14\ h\,\mathrm{Mpc}^{-1}$ and $Q_0$ in the range $0.14\ h\,\mathrm{Mpc}^{-1} \leq k < 0.3\ h\,\mathrm{Mpc}^{-1}$. Since the $k$-bins do not overlap between the two likelihoods, they are uncorrelated in the Gaussian limit. We fit the $P_{0,2,4}$ data vector with the one-loop effective field theory template of Refs. [3,11,14,34]. Note that we include the next-to-leading-order operator $\tilde{c}k^4\mu^4 P_{\mathrm{lin}}(k)$ in our analysis to account for higher-order FoG effects. Additionally, we use the full set of stochastic contributions from Refs. [34,47],

$$P_{\mathrm{stoch}}(k,\mu) = \left\{a_0\left(\frac{k}{k_{\mathrm{NL}}}\right)^2 + a_2\mu^2\left(\frac{k}{k_{\mathrm{NL}}}\right)^2 + P_{\mathrm{shot}}\right\} \cdot \frac{1}{\bar{n}}[\mathrm{Mpc}/h]^3, \tag{4.5}$$

where $\bar{n}$ is the inverse number density of tracers. Using the hexadecapole moment, we are able to break the strong degeneracy between $a_2$ and $\tilde{c}$, which is present in the $P_{0,2}$

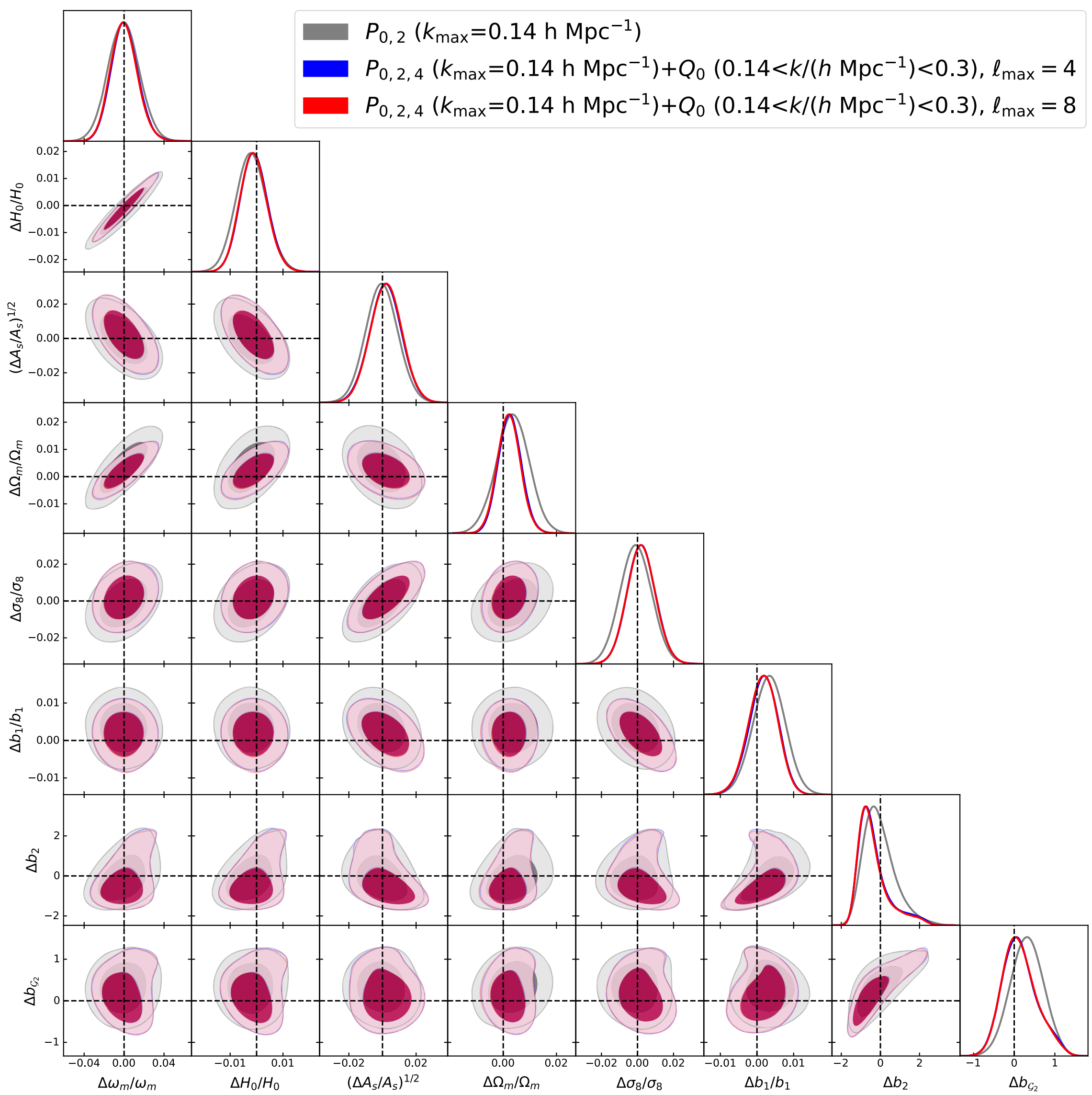


FIG. 3. Posteriors from the PT challenge data for the analysis with fixed $\Omega_b/\Omega_m$ and $n_s$.

TABLE I. Constraint on key cosmological and nuisance parameters from the PT challenge mock power spectra, obtained with fixed $\Omega_b/\Omega_m$ and $n_s$ as in Ref. [11]. $P_\ell$ denotes the data vector $\{P_0, P_2, P_4\}$ with $k_{\rm max} = 0.14\ h\,{\rm Mpc}^{-1}$. The second and third columns show results of the addition of $Q_0$ in the range $0.14 \leq k/(h{\rm Mpc}^{-1}) < 0.3$. In the third column, we add mean priors on the multipole moments with $\ell = 6$, 8 to the theory model. Parameters in the upper group part of the table were varied directly, while the lower group are the derived parameters.

| Parameter | $P_{0,2}$ ($k_{\rm max} = 0.14\ h\,{\rm Mpc}^{-1}$) | $P_\ell + Q_0$, $\ell_{\rm max} = 4$ | $P_\ell + Q_0$, $\ell_{\rm max} = 8$ |
|---|---|---|---|
| $\Delta H_0/H_0$ | $-0.0020 \pm 0.0059$ | $-0.00096 \pm 0.0052$ | $-0.0011 \pm 0.0052$ |
| $\Delta A^{1/2}/A^{1/2}$ | $-0.0004 \pm 0.0096$ | $0.0019 \pm 0.0093$ | $0.0021 \pm 0.0093$ |
| $\Delta\omega_m/\omega_m$ | $0.000 \pm 0.016$ | $0.001^{+0.013}_{-0.014}$ | $0.000^{+0.012}_{-0.014}$ |
| $\Delta b_1/b_1$ | $0.0033 \pm 0.0044$ | $0.0018^{+0.0041}_{-0.0037}$ | $0.0016 \pm 0.0040$ |
| $\Delta b_2$ | $-0.04^{+0.55}_{-0.96}$ | $-0.33^{+0.31}_{-0.93}$ | $-0.36^{+0.32}_{-0.90}$ |
| $\Delta b_{\mathcal{G}_2}$ | $0.31 \pm 0.41$ | $0.14^{+0.34}_{-0.50}$ | $0.14^{+0.34}_{-0.49}$ |
| $\Delta\Omega_m/\Omega_m$ | $0.0035 \pm 0.0062$ | $0.0025 \pm 0.0043$ | $0.0022 \pm 0.0044$ |
| $\Delta\sigma_8/\sigma_8$ | $-0.0008 \pm 0.0088$ | $0.0021 \pm 0.0079$ | $0.0021 \pm 0.0079$ |

likelihood. As to $Q_0$, we use the model (3.18), which depends on the same nuisance parameters as our likelihood for the multipoles for $k_{\rm max} = 0.14\ h/{\rm Mpc}$. We use the following parameter vector (see Ref. [14] for our notations):

$$\{\omega_m, h, A_s\} \times \{b_1, b_2, b_{\mathcal{G}_2}, b_{\Gamma_3}, c_0, c_2, c_4, \tilde{c}, a_0, a_2, P_{\rm shot}\}. \tag{4.6}$$

We fix $n_s$ and $\Omega_b/\Omega_m$ to the known fiducial values as in Ref. [11]. The following Gaussian priors on the nuisance parameters are assumed,

$$a_0 \sim \mathcal{N}(0, 1^2) \quad a_2 \sim \mathcal{N}(0, 1^2) \quad P_{\rm shot} \sim \mathcal{N}(0, 0.3^2),$$
$$b_{\Gamma_3} \sim \mathcal{N}\left(\frac{23}{42}(b_1 - 1), 1^2\right), \tag{4.7}$$

using flat infinite priors on $b_1$, $b_2$, $c_0$, $c_2$, $c_4$, $\tilde{c}$, and $b_{\mathcal{G}_2}$. The mean value of $b_{\Gamma_3}$ is taken from the prediction of the coevolution model [48,49]. Since the Poissonian shot-noise contribution was subtracted from the data, we assume that the mean residual contribution is zero, with variance corresponding to ~30% of $\bar{n}^{-1}$, consistent with the deviations due to the halo exclusions [13,50] expected for the BOSS-like host halos.

Let us now study the convergence of our method with respect to the value of the maximal multipolar index. In particular, we consider $\ell_{\rm max} = 4$, 6, 8. In all cases, the hexadecapole is fully included in the theory, data, and the covariance, with $\ell = 6$, 8 included only via priors. The results of our analysis are shown in Fig. 3 and Table I. Each parameter $p$ (except $b_2$ and $b_{\mathcal{G}_2}$) is shown in the format $\Delta p/p \equiv p/p_{\rm true} - 1$, where we use fiducial values for true cosmological parameters and extract the true value of $b_1$ from the galaxy-matter cross spectrum [11]. For $b_2$ and $b_{\mathcal{G}_2}$, we use the format $\Delta p \equiv p - p_{\rm true}$, where the true values of $b_2$ and $b_{\mathcal{G}_2}$ are measured from the combined power spectrum and bispectrum analysis [51]. For comparison, we show also the baseline results for the $P_{0,2}$ likelihood at $k_{\rm max} = 0.14\ h/{\rm Mpc}$. On the one hand, we can see that $Q_0$ narrows the contours for the $\omega_m$ and $H_0$ by $\lesssim 20\%$. This improvement is expected since these parameters are measured from the shape of $Q_0$. In contrast, the amplitude parameters $A^{1/2}$ and $\sigma_8$ cannot be accurately measured from the real-space galaxy power spectrum alone because of the degeneracy with galaxy bias. This explains why the posteriors for these parameters do not appreciably shrink after the inclusion of $Q_0$. The priors on higher order multipoles in the estimator $\check{Q}_0$ have a negligible effect on the posterior distribution, which motivates us to use $\ell_{\rm max} = 4$ as our baseline choice.

### B. Cosmological constraints with the $\omega_b$ prior

The information gain from $Q_0$ depends on the adopted priors and particular cosmological model. To illustrate this, we refitted the mock power spectra fixing $\omega_b$ instead of $\Omega_b/\Omega_m$, which was the choice adopted in our previous analysis. This simulates the addition of the $\omega_b$ prior, which is readily available in, e.g., Planck or big bang nucleosynthesis (BBN). We additionally allow $n_s$ to vary freely. The corresponding results are presented in Fig. 4 and in Table II. We find that the fit to $Q_0$ is unbiased all the way up to $k_{\rm max} = 0.4\ h\,{\rm Mpc}^{-1}$. We also see that in the case of a single prior on $\omega_b$ the addition of $Q_0$ improves the constraints on all the remaining cosmological parameters roughly by a factor of 2.

It is useful to compare our results with the case of the true real-space galaxy power spectrum, using the same $k$ ranges. To that end, we replace $Q_0$ with the actual real-space power spectrum $P_{\rm gg}$ extracted from the same PT challenge simulations and refit the data. The diagonal elements of the Gaussian covariance for $P_{\rm gg}$ are roughly four times smaller than similar elements of $Q_0$ for the same volume and shot noise. As a result of this small covariance, the

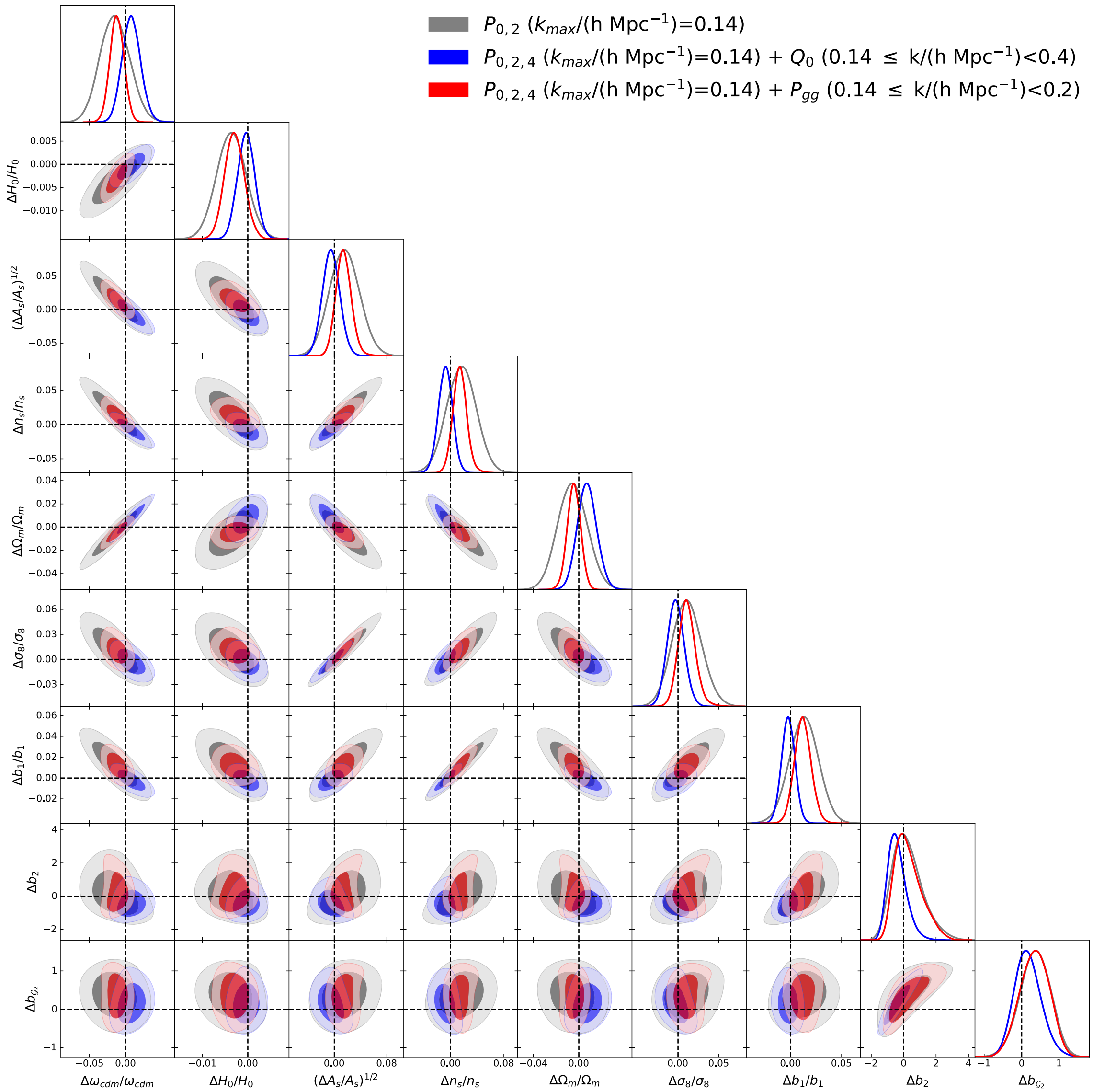


FIG. 4. Posteriors from the analysis of the PT challenge mock galaxy power spectrum with a prior on $\omega_b$.

TABLE II. Constraints from the analysis of the PT challenge data with the $\omega_b$ prior. $P_\ell$ denotes the data vector $\{P_0, P_2, P_4\}$ with $k_{\rm max} = 0.14\ h\,{\rm Mpc}^{-1}$. The second column shows results of the addition of $Q_0$ in the range $0.14 \le k/(h{\rm Mpc}^{-1}) < 0.4$, while in the third column, instead, we add the actual real-space power spectrum $P_{gg}(k)$ in the range $0.14 \le k/(h{\rm Mpc}^{-1}) < 0.2$.

| Parameter | $P_{0,2}, (k_{\rm max} = 0.14)$ | $P_\ell + Q_0(k_{\rm max} = 0.4)$ | $P_\ell + P_{\rm gg}(k_{\rm max} = 0.2)$ |
|---|---|---|---|
| $\Delta H_0/H_0$ | $-0.0036 \pm 0.0032$ | $-0.0004 \pm 0.0019$ | $-0.0029 \pm 0.0022$ |
| $\Delta A^{1/2}/A^{1/2}$ | $0.016 \pm 0.023$ | $-0.005 \pm 0.013$ | $0.014^{+0.011}_{-0.012}$ |
| $\Delta\omega_{\rm cdm}/\omega_{\rm cdm}$ | $-0.015 \pm 0.020$ | $0.008 \pm 0.013$ | $-0.0121 \pm 0.0096$ |
| $\Delta n_s/n_s$ | $0.016 \pm 0.022$ | $-0.008 \pm 0.011$ | $0.014 \pm 0.010$ |
| $\Delta b_1/b_1$ | $0.013 \pm 0.014$ | $-0.0024 \pm 0.0066$ | $0.0119 \pm 0.0082$ |
| $\Delta b_2$ | $0.25^{+0.70}_{-1.1}$ | $-0.40^{+0.42}_{-0.66}$ | $0.29^{+0.56}_{-1.0}$ |
| $\Delta b_{\mathcal{G}_2}$ | $0.36 \pm 0.40$ | $0.17^{+0.31}_{-0.39}$ | $0.34^{+0.41}_{-0.37}$ |
| $\Delta\Omega_m/\Omega_m$ | $-0.005 \pm 0.013$ | $0.0073 \pm 0.0085$ | $-0.0044 \pm 0.0059$ |
| $\Delta\sigma_8/\sigma_8$ | $0.011 \pm 0.018$ | $-0.003 \pm 0.010$ | $0.0110^{+0.0094}_{-0.011}$ |

one-loop perturbation theory fit to $P_{\rm gg}$ becomes biased beyond $k_{\rm max} = 0.2\ h\,{\rm Mpc}^{-1}$, which we adopt as a baseline data cut in this case. The resulted parameter limits are very similar to those obtained from our baseline $Q_0$ analysis at $k_{\rm max} = 0.4\ h\,{\rm Mpc}^{-1}$. This matches the expectation that the two statistics should be equivalent at the level of total information for appropriate data cuts.

## V. APPLICATIONS TO REALISTIC SURVEYS

So far, we have studied $Q_0$ in application to the PT challenge mocks whose total volume is 566 $h^{-3}\,{\rm Gpc}^3$ at the effective redshift $z = 0.61$. Current and future surveys will have somewhat smaller volumes; therefore, it is useful to test to what extent the real-space power spectrum can improve cosmological parameter measurements from realistic surveys. We address this question in this section and analyze the spectroscopic data from BOSS and DESI-like mock catalogs.

### A. BOSS survey

We apply now our method to the redshift-space galaxy power spectrum measurement of the BOSS survey [9]. Using the quadratic window-free estimator of Ref. [52], we measure the galaxy power spectrum multipoles of the BOSS data from four independent data chunks: low-$z$ ($z = 0.38$) north galactic cap (NGC), high-$z$ ($z = 0.61$) NGC, low-$z$ south galactic cap (SGC), and high-$z$ SGC [3,9]. For each chunk, we construct the likelihood as follows. We use the full $P_0$, $P_2$, $P_4$ moments up to $k_{\rm max} = 0.2\ h\,{\rm Mpc}^{-1}$ and $Q_0$, estimated with $\ell_{\rm max} = 4$, in the

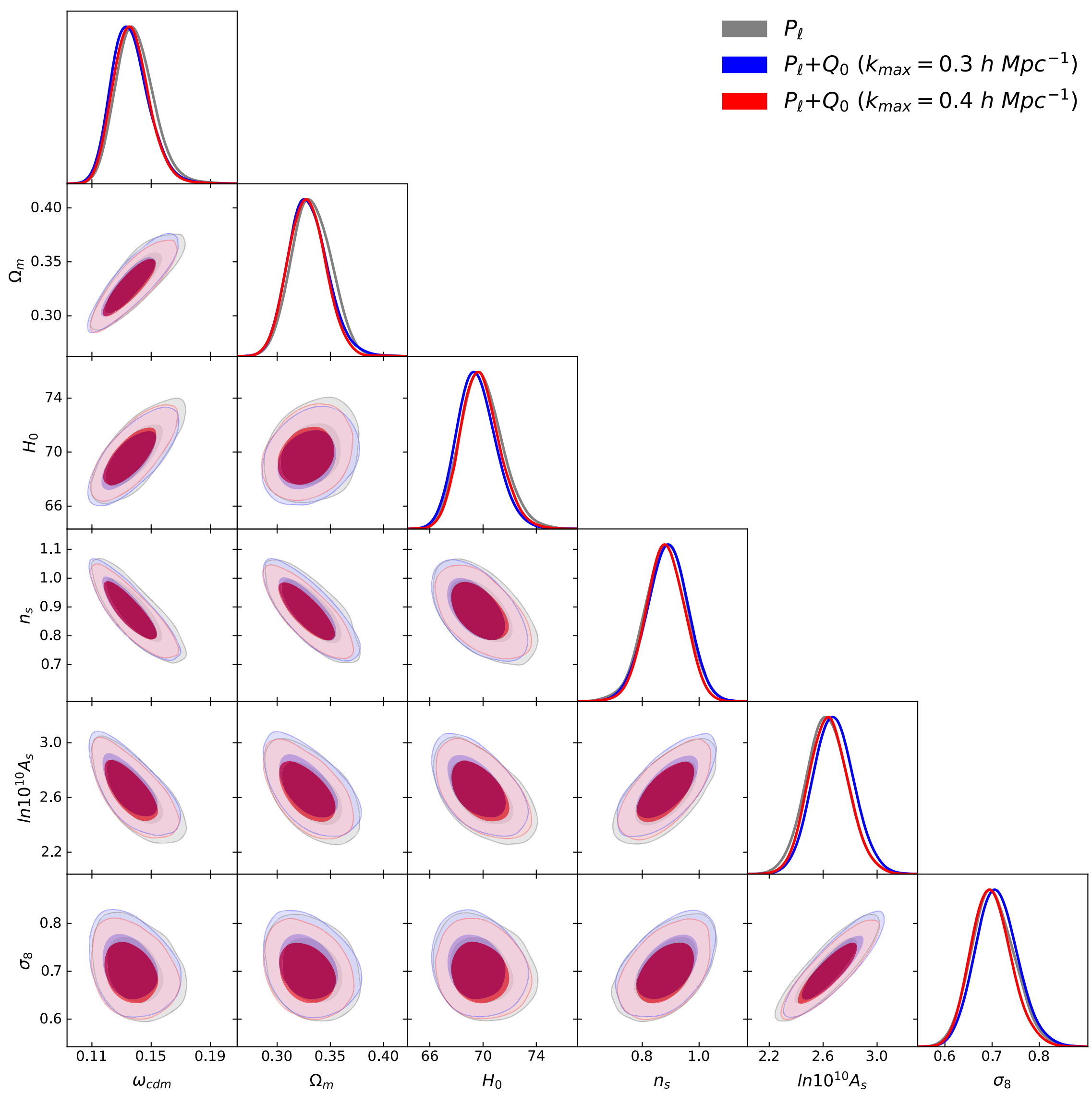


FIG. 5. Posteriors from the cosmological analysis of the BOSS galaxy power spectrum measurements combined with the BBN prior on $\omega_b$.

TABLE III. Cosmological parameter constraints from the BOSS data with the $\omega_b$ prior. $P_\ell$ denotes the $\ell = 0, 2, 4$ moments in the range $0.01 \leq k/(h\mathrm{Mpc}^{-1}) < 0.2$, and $Q_0$ is the real-space power spectrum within $0.2 \leq k/(h\mathrm{Mpc}^{-1}) < 0.3$ (third column) or $0.2 \leq k/(h\mathrm{Mpc}^{-1}) < 0.4$ (fourth column).

| Parameter | $P_\ell$ | $P_\ell + Q_0$ $(\frac{k_{\max}}{h\mathrm{Mpc}^{-1}} = 0.3)$ | $P_\ell + Q_0$ $(\frac{k_{\max}}{h\mathrm{Mpc}^{-1}} = 0.4)$ |
|---|---|---|---|
| $H_0/(\text{ km/s/Mpc})$ | $69.89^{+1.5}_{-1.7}$ | $69.51^{+1.3}_{-1.6}$ | $69.79^{+1.3}_{-1.6}$ |
| $\ln(10^{10}A_s)$ | $2.63^{+0.15}_{-0.16}$ | $2.68^{+0.15}_{-0.16}$ | $2.64^{+0.14}_{-0.16}$ |
| $\omega_{\rm cdm}$ | $0.139^{+0.011}_{-0.015}$ | $0.136^{+0.011}_{-0.014}$ | $0.137^{+0.011}_{-0.014}$ |
| $n_s$ | $0.883^{+0.076}_{-0.072}$ | $0.889^{+0.075}_{-0.07}$ | $0.881^{+0.07}_{-0.066}$ |
| $\Omega_m$ | $0.333^{+0.019}_{-0.02}$ | $0.329^{+0.017}_{-0.02}$ | $0.328^{+0.017}_{-0.019}$ |
| $\sigma_8$ | $0.704^{+0.044}_{-0.049}$ | $0.711^{+0.042}_{-0.049}$ | $0.699^{+0.04}_{-0.047}$ |

ranges $0.2\ h\,\mathrm{Mpc}^{-1} \leq k < 0.3\ h\,\mathrm{Mpc}^{-1}$ and $0.2\ h\,\mathrm{Mpc}^{-1} \leq k < 0.4\ h\,\mathrm{Mpc}^{-1}$. We do not include additional BAO data, as in Refs. [6,53,54], because we want to clearly assess the improvement from $Q_0$ with respect to the usual multipoles analysis.

We fit parameters of the minimal Lambda + cold dark matter model ($\Lambda$CDM) model assuming a single massive neutrino whose mass is fixed to 0.06 eV [55] and the BBN prior on the baryon density $\omega_b = 0.02258 \pm 0.0038$. We use the same priors on nuisance parameters as Ref. [53]. The covariance matrix for the full data vector is calculated using the empirical estimator based on 2048 Patchy mocks [56]. Our results for the joint fit of all four data chunks are displayed in Fig. 5 and in Table III,[2] where we show results from the usual redshift-space multipoles alone and with $Q_0$, taken at $k_{\max} = 0.3\ h\,\mathrm{Mpc}^{-1}$ and $0.4\ h\,\mathrm{Mpc}^{-1}$.

In this case, the inclusion of $Q_0$ leads to somewhat marginal improvements of $\sim$10%, which are barely visible in the triangle plot. This is a result of a relatively large shot-noise level of the BOSS galaxy sample, $\bar{n}^{-1} \simeq (3-5)\times 10^3\ h^{-3}\,\mathrm{Mpc}^3$. In order to illustrate this, we may analyze mocks with lower shot noise, as appropriate for the upcoming DESI survey.

### B. DESI-like emission line galaxy mocks

In order to estimate the performance of our method for surveys such as Euclid and DESI, we apply it to the analysis of the mock emission line galaxy (ELG) catalogs from the extended Baryon Acoustic Oscillation Survey (eBOSS) survey [57]. These mocks simulate the clustering of the ELGs, which exhibit a weaker fingers of God signature than the BOSS LRG sample [54], so the $P_\ell$ analysis is valid up to higher $k_{\max}$ in this case. On the one hand, this factor suggests that the improvement from $Q_0$ may be somewhat less sizable than the improvement that we expect from the LRG samples. On the other hand, this sample has lower shot noise, and hence the inclusion of $Q_0$ might be more beneficial here. To understand which effect takes over, we need a quantitative comparison with reliable mocks, such as those recently produced using the Outer Rim simulation.

These eBOSS ELG mocks are based on the Outer Rim dark matter simulation [58], which were populated with ELG mock galaxies according to the eBOSS ELG clustering measurements [59]. We use the HOD-3 mock catalogs at $z = 0.865$. We combine the 27 publicly available sub-boxes into one large box from which we measure the mock redshift-space power spectrum multipoles.[3] The mocks have the following fiducial $\Lambda$CDM cosmology:

$$h = 0.71, \qquad \omega_{\rm cdm} = 0.1109, \qquad \omega_b = 0.02258,$$
$$n_s = 0.963, \qquad \sigma_8 = 0.8, \qquad M_{\rm tot} = 0\ \mathrm{eV}. \tag{5.1}$$

We compare three different analyses: fits to $\ell = 0, 2, 4$ moments at $k_{\max} = 0.2\ h\,\mathrm{Mpc}^{-1}$, fits to $\ell = 0, 2, 4$ moments at $k_{\max} = 0.2\ h\,\mathrm{Mpc}^{-1}$ and $Q_0$ for $0.2\ h\,\mathrm{Mpc}^{-1} \leq k < 0.3\ h\,\mathrm{Mpc}^{-1}$, and fits to $\ell = 0, 2, 4$ moments at $k_{\max} = 0.2\ h\,\mathrm{Mpc}^{-1}$ and $Q_0$ for $0.2\ h\,\mathrm{Mpc}^{-1} \leq k < 0.4\ h\,\mathrm{Mpc}^{-1}$. We compute the covariance in the Gaussian approximation using the true shot-noise value $\bar{n}^{-1} \simeq 500\ h^{-3}\,\mathrm{Mpc}^3$ and the total volume of $V = 27\ h^{-3}\,\mathrm{Gpc}^3$, similar to the DESI ELG volume [60]. We use the same priors on nuisance parameters as in Ref. [54] but vary the spectral index $n_s$ in the fit in addition to $h$, $\Omega_m$, and $A_s$. The physical baryon density $\omega_b$ is fixed to the fiducial value of the simulation.

Our results are shown in Fig. 6 and in Table IV. First, all true cosmological parameters are recovered within 68% confidence limits. Second, we see that the inclusion

[2]Only the parameters that are well constrained by the data, i.e., not dominated by priors, are shown in this table.

[3]The public data on ELG mocks (based on the Outer Rim snapshots) is given in the form of subcatalogs extracted from 27 nonoverlapping sub-boxes, which were cut from the original Outer Rim box. In the previous version of this paper, we measured the power spectrum from each sub-box, incorrectly assuming periodic boundary conditions. This has generated a bias in the $\Omega_m$ recovery. The bias disappears when the power spectrum is measured from the cumulative catalog produced by a proper combination of the sub-boxes, as presented above.

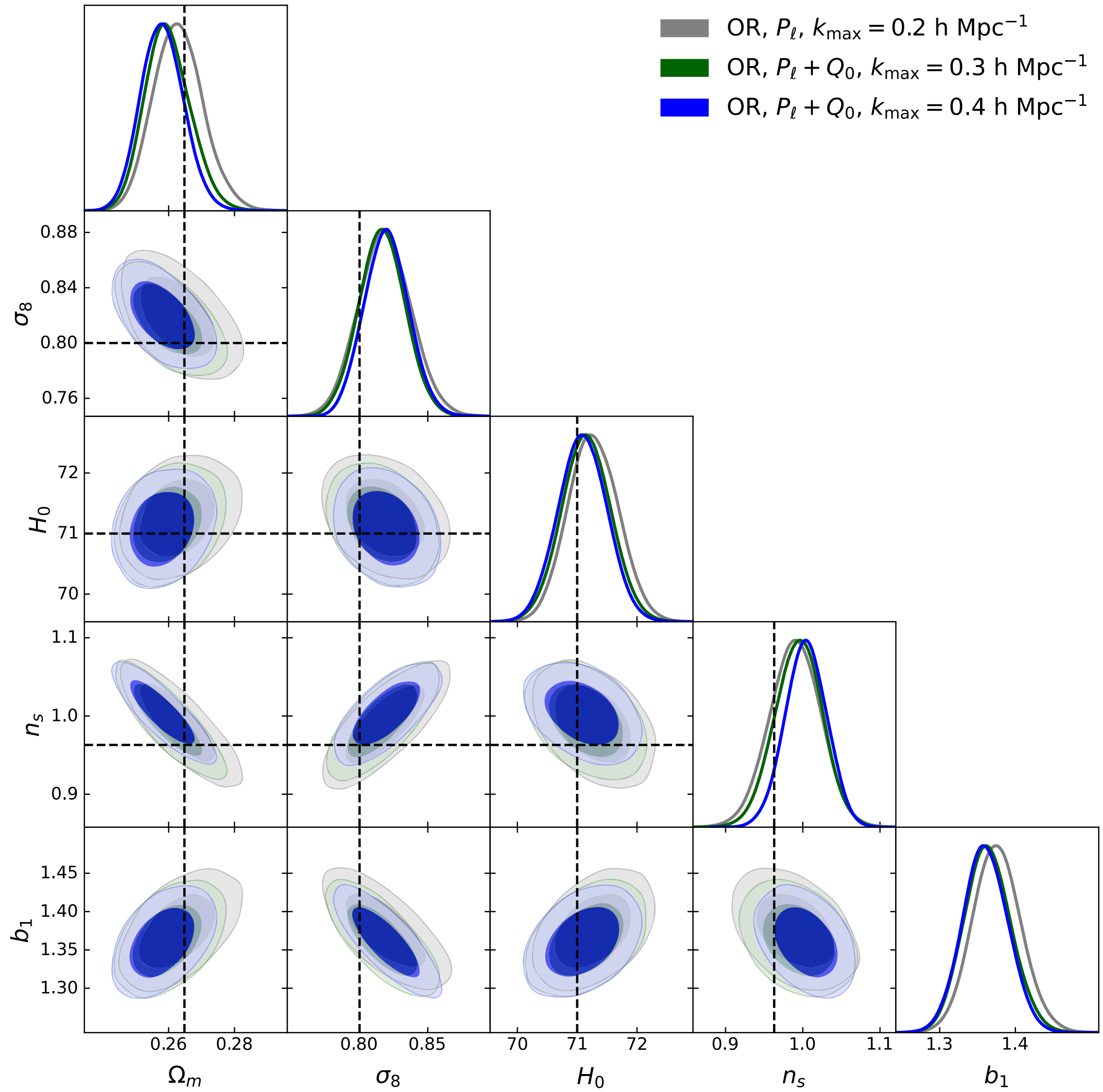


FIG. 6. Posteriors from the cosmological analysis of the Outer Rim (OR) emission line galaxy mock power spectrum measurements.

of $Q_0$ shrinks the one-dimensional marginalized contours for $\Omega_m$ and $n_s$ by ~20%. Third, the posteriors do not significantly shrink when the data cut for $Q_0$ is increased from 0.3 $h\,\mathrm{Mpc}^{-1}$ to 0.4 $h\,\mathrm{Mpc}^{-1}$. This implies that cosmological information in the real-space power spectrum is limited even for low shot-noise samples.

TABLE IV. Constraints from the analysis of the Outer Rim mock data with the $\omega_b$ prior. We show only the parameters that are well constrained by the data. For $P_\ell$, the data cut is $k_{max} = 0.2\ h\,\mathrm{Mpc}^{-1}$ in all analyses. For $Q_0$, we use the ranges $0.2\ h\,\mathrm{Mpc}^{-1} \leq k < 0.3\ h\,\mathrm{Mpc}^{-1}$ (middle column) and $0.2\ h\,\mathrm{Mpc}^{-1} \leq k < 0.4\ h\,\mathrm{Mpc}^{-1}$ (right column).

| Parameter | $P_\ell$ | $P_\ell + Q_0, (k_{max} = 0.3)$ | $P_\ell + Q_0, (k_{max} = 0.4)$ |
|---|---|---|---|
| $H_0$ (km/s/Mpc) | $71.27^{+0.43}_{-0.43}$ | $71.15^{+0.41}_{-0.42}$ | $71.09^{+0.42}_{-0.42}$ |
| $\ln(10^{10}A_s)$ | $3.094^{+0.066}_{-0.068}$ | $3.111^{+0.065}_{-0.062}$ | $3.125^{+0.061}_{-0.063}$ |
| $\omega_{cdm}$ | $0.111^{+0.0043}_{-0.0048}$ | $0.109^{+0.0039}_{-0.0045}$ | $0.1079^{+0.0037}_{-0.0043}$ |
| $n_s$ | $0.9896^{+0.034}_{-0.033}$ | $0.9944^{+0.032}_{-0.03}$ | $1.004^{+0.028}_{-0.028}$ |
| $b_1$ | $1.375^{+0.031}_{-0.034}$ | $1.364^{+0.031}_{-0.033}$ | $1.36^{+0.03}_{-0.031}$ |
| $\Omega_m$ | $0.263^{+0.0071}_{-0.0081}$ | $0.2598^{+0.0064}_{-0.0076}$ | $0.2581^{+0.0064}_{-0.0069}$ |
| $\sigma_8$ | $0.8185^{+0.019}_{-0.02}$ | $0.8165^{+0.017}_{-0.017}$ | $0.8198^{+0.016}_{-0.017}$ |

All in all, we see that the improvement from $Q_0$ in the case of DESI-like mocks with high number density is quite significant. Therefore, the $Q_0$ statistic can be an important statistic for future surveys.

## VI. CONCLUSIONS

In this paper, we have proposed a new statistic, dubbed $Q_0$, which acts as a proxy for the real-space power spectrum and can be used to mitigate the impact of fingers of God. This can be easily constructed from the conventional redshift-space power spectrum Legendre multipoles. We have shown how to perform such a reconstruction for an arbitrary survey and systematically include the information from higher-order Legendre multipoles if they carry non-negligible signal. Using our approach, $Q_0$ and its covariance matrix can be trivially computed from theory or mock catalogs and included in the analysis at negligible extra cost. We have shown that the addition of $Q_0$ leads to notable improvements on cosmological constraints from mock catalogs, the amplitude of which varies within $(10-100)\%$ depending on survey characteristics, the choice of parameters, and priors in a particular analysis.

It is useful to compare $Q_0$ to the two-dimensional redshift-space power spectrum $P(k,\mu)$. In terms of the signal-to-noise ratio, at $k_{\max}=0.3\ h\,\mathrm{Mpc}^{-1}$, the transverse moment $Q_0$ contains the same signal as $P(k,\mu)$ in the range $|\mu|\in[0,0.3]$. Thus, we expect information gains from $Q_0$ to be roughly equivalent the corresponding $\mu$-wedge. Given that the remaining $\mu$-modes are quite sensitive to fingers of God, we expect that the $|\mu|$-range [0.3, 1] contains very little, if any, viable cosmological information.

Crucially, $Q_0$ is more economic than $P(k,\mu)$, as it captures all relevant cosmological information in a relatively condensed data vector. This allows us to reduce the dimensionality of the total data vector compared to the $P(k,\mu)$ case, an effort which is of use if one wishes to avoid sampling noise biases if the covariance matrix is estimated from mock catalogs [61]. Alternative ways of avoiding this issue include analytic covariance matrix calculation [46,62] or subspace-projection techniques [63].

The information gain from the addition of $Q_0$ for future surveys depends on several factors. First and foremost, it is dependent on the strength of FoG. The effect is large for the BOSS-like luminous red galaxies [3,9] and the bright galaxy sample to be observed by DESI [60], though less so for emission line galaxies. Hence, we expect $Q_0$ to be particularly useful for the former galaxy selections.

The second factor determining the usefulness of $Q_0$ is the particular theoretical model chosen to fit the data and adopted priors. We have found that within Lambda + cold dark matter + massive neutrinos model ($\nu\Lambda$CDM) the improvement from $Q_0$ increases when less restrictive priors are used and more free parameters are kept in the fit. Therefore, we expect even more information gain for models beyond $\Lambda$CDM, e.g., for the early dark energy scenario (see, e.g., Ref. [64] and references therein), models with neutrino masses and additional relativistic degrees of freedom [4], axion dark matter cosmologies [65], or dynamical dark energy models [53,66].

Our work can be extended in several ways. First, the transverse modes measured in a realistic survey can be contaminated by systematics [39,54], so it is important to study to what extend this systematics can be mitigated in a realistic survey. Second, it would be interesting to see how much $Q_0$ can improve the constraints in combination with other techniques, such as the bispectrum and the BAO postreconstruction information. This study can be performed for different tracers and within different cosmological models. Finally, it will be interesting to work out an extension of our formalism to higher-order statistics. We leave these research directions for future work.

## ACKNOWLEDGMENTS

We thank the anonymous referee for pointing out to a potential issue with the fit to the Outer Rim eBOSS ELG mocks, which motivated us to revisit our analysis and to eventually fix the error that was causing the bias in the fit. We thank Marcel Schmittfull for his collaboration at the initial stage of this project. The work of M. I. has been supported by NASA through NASA Hubble Fellowship Grant No. HST-HF2-51483.001-A awarded by the Space Telescope Science Institute, which is operated by the Association of Universities for Research in Astronomy, Inc., under NASA Contract No. NAS5-26555. O. P. thanks the Simons Foundation for additional support. This work was supported in part by MEXT/JSPS KAKENHI Grants No. JP19H00677, No. JP20H05861, and No. JP21H01081. We also acknowledge financial support from Japan Science and Technology Agency (JST) AIP Acceleration Research Grant No. JP20317829. The simulation data analysis was performed partly on Cray XC50 at Center for Computational Astrophysics, National Astronomical Observatory of Japan.

## APPENDIX: GENERAL RELATION BETWEEN MOMENTS AND MULTIPOLES

The general relationship between power spectrum multipoles $P_{2n}$ and moments $Q_{2m}$ can be derived as follows. The power spectrum $P(k,\mu)$ can be represented by an expansion in even Legendre polynomials $\mathcal{L}_{2n}$ or in even powers of $\mu$:

$$P(k,\mu)=\sum_{n=0}^{\infty}P_{2n}(k)\mathcal{L}_{2n}(\mu) \tag{A1}$$

$$=\sum_{m=0}^{\infty}Q_{2m}(k)\mu^{2m}. \tag{A2}$$

They are related by

$$P_{2n}(k) = \frac{4n+1}{2}\int_{-1}^{1} \mathrm{d}\mu\, P(k,\mu)\mathcal{L}_{2n}(\mu) \tag{A3}$$

$$= \sum_{m=n}^{\infty} M_{nm} Q_{2m}(k), \tag{A4}$$

where $M$ is an upper triangular matrix given by

$$M_{nm} = \begin{cases} \frac{(4n+1)(2m)!}{2^{m-n}(m-n)!(2n+2m+1)!!}, & m \geq n, \\ 0 & \text{else}. \end{cases} \tag{A5}$$

This follows by expressing powers of $\mu$ in terms of Legendre polynomials. If Eqs. (A1) and (A2) can be truncated at a finite $n_{\max} = m_{\max}$, then the equations relating moments and multipoles are a finite linear system of equations, and $M$ is a $n_{\max} \times n_{\max}$ matrix. Under that assumption, the moments in terms of multipoles are

$$\mathbf{Q}(k) = M^{-1}\mathbf{P}(k) \tag{A6}$$

or explicitly

$$Q_{2m}(k) = \sum_{n=m}^{n_{\max}} (M^{-1})_{mn} P_{2n}(k). \tag{A7}$$

In particular, the $\mu^0$ part of $P(k,\mu)$ is a sum over all nonzero multipoles,

$$Q_0(k) = \sum_{n=0}^{n_{\max}} (M^{-1})_{0n} P_{2n}(k). \tag{A8}$$

As discussed in the main text, care must be taken when the measured power spectrum multipoles are noisy.


[1] F. Beutler (BOSS Collaboration) *et al.*, The clustering of galaxies in the completed SDSS-III Baryon Oscillation Spectroscopic Survey: Anisotropic galaxy clustering in Fourier-space, Mon. Not. R. Astron. Soc. **466**, 2242 (2017).

[2] A. Chudaykin and M. M. Ivanov, Measuring neutrino masses with large-scale structure: Euclid forecast with controlled theoretical error, J. Cosmol. Astropart. Phys. 11 (2019) 034.

[3] M. M. Ivanov, M. Simonovic, and M. Zaldarriaga, Cosmological parameters from the BOSS galaxy power spectrum, J. Cosmol. Astropart. Phys. 05 (2020) 042.

[4] M. M. Ivanov, M. Simonović, and M. Zaldarriaga, Cosmological parameters and neutrino masses from the final Planck and full-shape BOSS data, Phys. Rev. D **101**, 083504 (2020).

[5] T. Colas, G. D'amico, L. Senatore, P. Zhang, and F. Beutler, Efficient cosmological analysis of the SDSS/BOSS data from the effective field theory of large-scale structure, J. Cosmol. Astropart. Phys. 06 (2020) 001.

[6] O. H. E. Philcox, M. M. Ivanov, M. Simonović, and M. Zaldarriaga, Combining full-shape and BAO analyses of galaxy power spectra: A 1.6% CMB-independent constraint on H0, J. Cosmol. Astropart. Phys. 05 (2020) 032.

[7] O. H. Philcox, B. D. Sherwin, G. S. Farren, and E. J. Baxter, Determining the Hubble constant without the sound horizon: Measurements from galaxy surveys, Phys. Rev. D **103**, 023538 (2021).

[8] N. Sailer, E. Castorina, S. Ferraro, and M. White, Cosmology at high redshift—a probe of fundamental physics, J. Cosmol. Astropart. Phys. 12 (2021) 049.

[9] S. Alam (BOSS Collaboration) *et al.*, The clustering of galaxies in the completed SDSS-III Baryon Oscillation Spectroscopic Survey: Cosmological analysis of the DR12 galaxy sample, Mon. Not. R. Astron. Soc. **470**, 2617 (2017).

[10] J. C. Jackson, Fingers of God: A critique of Rees' theory of primordial gravitational radiation, Mon. Not. R. Astron. Soc. **156**, 1P (1972).

[11] T. Nishimichi, G. D'Amico, M. M. Ivanov, L. Senatore, M. Simonovic, M. Takada, M. Zaldarriaga, and P. Zhang, Blinded challenge for precision cosmology with large-scale structure: Results from effective field theory for the redshift-space galaxy power spectrum, Phys. Rev. D **102**, 123541 (2020).

[12] G. D'Amico, J. Gleyzes, N. Kokron, D. Markovic, L. Senatore, P. Zhang, F. Beutler, and H. Gil-Marín, The cosmological analysis of the SDSS/BOSS data from the effective field theory of large-scale structure, J. Cosmol. Astropart. Phys. 05 (2020) 005.

[13] M. Schmittfull, M. Simonović, V. Assassi, and M. Zaldarriaga, Modeling biased tracers at the field level, Phys. Rev. D **100**, 043514 (2019).

[14] A. Chudaykin, M. M. Ivanov, O. H. E. Philcox, and M. Simonović, Nonlinear perturbation theory extension of the Boltzmann code CLASS, Phys. Rev. D **102**, 063533 (2020).

[15] Z. Vlah, M. White, and A. Aviles, A Lagrangian effective field theory, J. Cosmol. Astropart. Phys. 09 (2015) 014.

[16] Z. Vlah and M. White, Exploring redshift-space distortions in large-scale structure, J. Cosmol. Astropart. Phys. 03 (2019) 007.

[17] S.-F. Chen, Z. Vlah, and M. White, Consistent modeling of velocity statistics and redshift-space distortions in one-loop perturbation theory, J. Cosmol. Astropart. Phys. 07 (2020) 062.

[18] S.-F. Chen, Z. Vlah, E. Castorina, and M. White, Redshift-space distortions in Lagrangian perturbation theory, J. Cosmol. Astropart. Phys. 03 (2021) 100.

[19] E. A. Kazin, A. G. Sanchez, and M. R. Blanton, Improving measurements of H(z) and Da(z) by analyzing clustering anisotropies, Mon. Not. R. Astron. Soc. **419**, 3223 (2012).

[20] J. N. Grieb (BOSS Collaboration) *et al.*, The clustering of galaxies in the completed SDSS-III Baryon Oscillation Spectroscopic Survey: Cosmological implications of the Fourier space wedges of the final sample, Mon. Not. R. Astron. Soc. **467**, 2085 (2017).

[21] M. Tegmark, A. J. S. Hamilton, and Y.-Z. Xu, The power spectrum of galaxies in the 2dF 100k redshift survey, Mon. Not. R. Astron. Soc. **335**, 887 (2002).

[22] M. Tegmark (SDSS Collaboration) *et al.*, The 3-D power spectrum of galaxies from the SDSS, Astrophys. J. **606**, 702 (2004).

[23] B. A. Reid, D. N. Spergel, and P. Bode, Luminous red galaxy halo density field reconstruction and application to large scale structure measurements, Astrophys. J. **702**, 249 (2009).

[24] A. J. S. Hamilton and M. Tegmark, The Real space power spectrum of the PSCz survey from 0.01 to 300 h $Mpc^{-1}$, Mon. Not. R. Astron. Soc. **330**, 506 (2002).

[25] R. Scoccimarro, Redshift-space distortions, pairwise velocities, and nonlinearities, Phys. Rev. D **70**, 083007 (2004).

[26] T. Baldauf, M. Mirbabayi, M. Simonović, and M. Zaldarriaga, LSS constraints with controlled theoretical uncertainties, arXiv:1602.00674.

[27] A. Chudaykin, M. M. Ivanov, and M. Simonović, Optimizing large-scale structure data analysis with the theoretical error likelihood, Phys. Rev. D **103**, 043525 (2021).

[28] T. Brinckmann and J. Lesgourgues, MONTEPYTHON 3: Boosted MCMC sampler and other features, Phys. Dark Universe **24**, 100260 (2019).

[29] B. Audren, J. Lesgourgues, K. Benabed, and S. Prunet, Conservative constraints on early cosmology: An illustration of the Monte Python cosmological parameter inference code, J. Cosmol. Astropart. Phys. 02 (2013) 001.

[30] A. Lewis, GetDist: A PYTHON package for analysing Monte Carlo samples, arXiv:1910.13970.

[31] N. Kaiser, Clustering in real space and in redshift space, Mon. Not. R. Astron. Soc. **227**, 1 (1987).

[32] L. Senatore and M. Zaldarriaga, Redshift space distortions in the effective field theory of large scale structures, arXiv:1409.1225.

[33] M. Lewandowski, L. Senatore, F. Prada, C. Zhao, and C.-H. Chuang, EFT of large scale structures in redshift space, Phys. Rev. D **97**, 063526 (2018).

[34] A. Perko, L. Senatore, E. Jennings, and R. H. Wechsler, Biased tracers in redshift space in the EFT of large-scale structure, arXiv:1610.09321.

[35] D. Baumann, A. Nicolis, L. Senatore, and M. Zaldarriaga, Cosmological non-linearities as an effective fluid, J. Cosmol. Astropart. Phys. 07 (2012) 051.

[36] J. J. M. Carrasco, M. P. Hertzberg, and L. Senatore, The effective field theory of cosmological large scale structures, J. High Energy Phys. 09 (2012) 082.

[37] K. Yamamoto, M. Nakamichi, A. Kamino, B. A. Bassett, and H. Nishioka, A measurement of the quadrupole power spectrum in the clustering of the 2dF QSO survey, Publ. Astron. Soc. Jpn. **58**, 93 (2006).

[38] R. Scoccimarro, Fast estimators for redshift-space clustering, Phys. Rev. D **92**, 083532 (2015).

[39] N. Hand, Y. Li, Z. Slepian, and U. Seljak, An optimal FFT-based anisotropic power spectrum estimator, J. Cosmol. Astropart. Phys. 07 (2017) 002.

[40] C. Alcock and B. Paczynski, An evolution free test for non-zero cosmological constant, Nature (London) **281**, 358 (1979).

[41] M. M. Ivanov and S. Sibiryakov, Infrared resummation for biased tracers in redshift space, J. Cosmol. Astropart. Phys. 07 (2018) 053.

[42] T. Baldauf, M. Mirbabayi, M. Simonović, and M. Zaldarriaga, Equivalence principle and the Baryon acoustic peak, Phys. Rev. D **92**, 043514 (2015).

[43] D. Blas, S. Floerchinger, M. Garny, N. Tetradis, and U. A. Wiedemann, Large scale structure from viscous dark matter, J. Cosmol. Astropart. Phys. 11 (2015) 049.

[44] D. Blas, M. Garny, M. M. Ivanov, and S. Sibiryakov, Time-sliced perturbation theory II: Baryon acoustic oscillations and infrared resummation, J. Cosmol. Astropart. Phys. 07 (2016) 028.

[45] A. Vasudevan, M. M. Ivanov, S. Sibiryakov, and J. Lesgourgues, Time-sliced perturbation theory with primordial non-Gaussianity and effects of large bulk flows on inflationary oscillating features, J. Cosmol. Astropart. Phys. 09 (2019) 037.

[46] D. Wadekar, M. M. Ivanov, and R. Scoccimarro, Cosmological constraints from BOSS with analytic covariance matrices, Phys. Rev. D **102**, 123521 (2020).

[47] M. Schmittfull, M. Simonović, M. M. Ivanov, O. H. E. Philcox, and M. Zaldarriaga, Modeling galaxies in redshift space at the field level, J. Cosmol. Astropart. Phys. 05 (2021) 059.

[48] V. Desjacques, D. Jeong, and F. Schmidt, Large-scale galaxy bias, Phys. Rep. **733**, 1 (2018).

[49] M. M. Abidi and T. Baldauf, Cubic halo bias in Eulerian and Lagrangian space, J. Cosmol. Astropart. Phys. 07 (2018) 029.

[50] T. Baldauf, U. S. Seljak, R. E. Smith, N. Hamaus, and V. Desjacques, Halo stochasticity from exclusion and non-linear clustering, Phys. Rev. D **88**, 083507 (2013).

[51] M. M. Ivanov, O. H. E. Philcox, T. Nishimichi, M. Simonović, M. Takada, and M. Zaldarriaga, Precision analysis of the redshift-space galaxy bispectrum, arXiv:2110.10161.

[52] O. H. E. Philcox, Cosmology without window functions: Quadratic estimators for the galaxy power spectrum, Phys. Rev. D **103**, 103504 (2021).

[53] A. Chudaykin, K. Dolgikh, and M. M. Ivanov, Constraints on the curvature of the Universe and dynamical dark energy from the full-shape and BAO data, Phys. Rev. D **103**, 023507 (2021).

[54] M. M. Ivanov, Cosmological constraints from the power spectrum of eBOSS emission line galaxies, Phys. Rev. D **104**, 103514 (2021).

[55] N. Aghanim (Planck Collaboration) *et al.*, Planck 2018 results. VI. Cosmological parameters, Astron. Astrophys. **641**, A6 (2020).

[56] F.-S. Kitaura *et al.*, The clustering of galaxies in the SDSS-III Baryon Oscillation Spectroscopic Survey: Mock galaxy catalogues for the BOSS Final Data Release, Mon. Not. R. Astron. Soc. **456**, 4156 (2016).

[57] S. Alam *et al.*, The completed SDSS-IV extended Baryon Oscillation Spectroscopic Survey: N-body mock challenge for the eBOSS emission line galaxy sample, arXiv:2007.09004.

[58] K. Heitmann *et al.*, The outer rim simulation: A path to many-core supercomputers, Astrophys. J. Suppl. Ser. **245**, 16 (2019).

[59] S. Avila *et al.*, The Completed SDSS-IV extended Baryon Oscillation Spectroscopic Survey: Exploring the halo occupation distribution model for emission line galaxies, Mon. Not. R. Astron. Soc. **499**, 5486 (2020).

[60] A. Aghamousa *et al.* (DESI Collaboration), The DESI experiment part I: Science, targeting, and survey design, arXiv:1611.00036.

[61] W. J. Percival *et al.*, The clustering of Galaxies in the SDSS-III Baryon Oscillation Spectroscopic Survey: Including covariance matrix errors, Mon. Not. R. Astron. Soc. **439**, 2531 (2014).

[62] D. Wadekar and R. Scoccimarro, The galaxy power spectrum multipoles covariance in perturbation theory, Phys. Rev. D **102**, 123517 (2020).

[63] O. H. E. Philcox, M. M. Ivanov, M. Zaldarriaga, M. Simonovic, and M. Schmittfull, Fewer mocks and less noise: Reducing the dimensionality of cosmological observables with subspace projections, Phys. Rev. D **103**, 043508 (2021).

[64] M. M. Ivanov, E. McDonough, J. C. Hill, M. Simonović, M. W. Toomey, S. Alexander, and M. Zaldarriaga, Constraining early dark energy with large-scale structure, Phys. Rev. D **102**, 103502 (2020).

[65] A. Laguë, J. R. Bond, R. Hložek, K. K. Rogers, D. J. E. Marsh, and D. Grin, Constraining ultralight axions with galaxy surveys, arXiv:2104.07802.

[66] G. D'Amico, L. Senatore, and P. Zhang, Limits on *w*CDM from the EFT of LSS with the PyBird code, J. Cosmol. Astropart. Phys. 01 (2021) 006.